

ECM-OPCC: Efficient Context Model for Octree-based Point Cloud Compression

Yiqi Jin^{1,2*}, Ziyu Zhu³, Tongda Xu¹, Yuhuan Lin^{1,2}, Yan Wang^{1†}

¹Institute for AI Industry Research (AIR), Tsinghua University

²Department of Automation, Tsinghua University

³Department of Computer Science, Tsinghua University

Abstract

Recently, deep learning methods have shown promising results in point cloud compression. For octree-based point cloud compression, previous works show that the information of ancestor nodes and sibling nodes are equally important for predicting current node. However, those works either adopt insufficient context or bring intolerable decoding complexity (e.g. > 600 s). To address this problem, we propose a sufficient yet efficient context model and design an efficient deep learning codec for point clouds. Specifically, we first propose a window-constrained multi-group coding strategy to exploit the autoregressive context while maintaining decoding efficiency. Then, we propose a dual transformer architecture to utilize the dependency of current node on its ancestors and siblings. We also propose a random-masking pre-train method to enhance our model. Experimental results show that our approach achieves state-of-the-art performance for both lossy and lossless point cloud compression. Moreover, our multi-group coding strategy saves 98% decoding time compared with previous octree-based compression method.

1 Introduction

Recently, Deep Point Cloud Compression (DPCC) has outperformed traditional hand-crafted codec (Fu et al. 2022). Inspired by learned image compression and traditional point cloud codec, deep learning community invents tree-based, voxel-based, projection-based and point-based compression algorithms: Tree-based approach represents point cloud by octree (Huang et al. 2020) and aggregates ancestor and sibling information to predict current node occupancy; Voxel-based approach quantizes point cloud into voxel grid (Que, Lu, and Xu 2021) and uses 3D convolution as learned transform; Projection-based approach (Tu et al. 2019) projects 3D point cloud to 2D image and uses image compression techniques to compress it; And point-based approach (You and Gao 2021) utilizes modules from point cloud understanding (Liang and Liang 2022) to transform point cloud and compress transformed points and features. Among above-mentioned methods, octree-based approach is commonly used for large scale sparse point cloud (Cao, Preda, and Zaharia 2019).

*This work is done when Yiqi Jin and Yuhuan Lin are interns at AIR, Tsinghua University

†Yan Wang is the corresponding author.

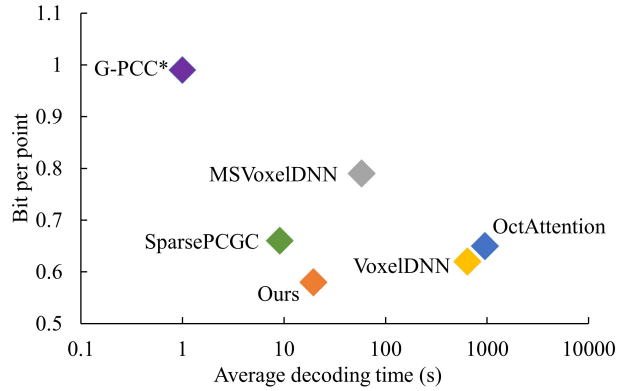


Figure 1: The bpp-decoding time of different methods. Our method achieves SOTA bpp while shows faster or comparable decoding time compared with other deep learning methods. *G-PCC is traditional non-deep learning method.

A major issue of octree-based methods is the decoding complexity due to the autoregressive context model. For example, in Fu et al. (2022), both ancestor and sibling information are introduced as autoregressive context models, which greatly increases the decoding complexity. Inspired by parallel autoregressive density estimation (Reed et al. 2017), we propose to solve this problem by multi-group coding strategy. Specifically, we factorize the fully autoregressive context of Fu et al. (2022) into layer-wise autoregressive context, and slice the nodes within the layers into parallel-decodable context window. Within each window, we deploy group-wise autoregressive context. Furthermore, we propose a dual transformer architecture to process branches containing ancestor and sibling information. Besides, we also introduce random masking pre-training strategy to boost performance of our context model. Experimental results show that our proposed method outperforms previous deep point cloud compression methods in both compression ratio and decoding time.

Our main contributions are as follows:

- We propose a multi-group coding strategy that enables parallel decoding of nodes inside each context window, which greatly accelerates decoding process while main-

taining compression performance.

- We develop a dual transformer with level-parallel and group-parallel branch to better extract context information from ancestors and siblings.
- We introduce randomly masking input occupancy code as an efficient pre-training strategy to boost performance of our context model.
- Our proposed model achieves SOTA bitrate for lossless compression and R-D (Rate-Distortion) performance for lossy compression. Moreover, it saves 98% decoding time compared with previous works.

2 Related Work

2.1 Octree-based DPCC

Octree-based approaches (Huang et al. 2020; Biswas et al. 2020) represent point cloud by octree data structure and convert point cloud compression to lossless tree structure compression. Specifically, OctSqueeze (Huang et al. 2020) uses deep recurrent model to aggregate ancestral information inside octree to predict occupancy of children node. MuSCLE (Biswas et al. 2020) improves this work by introducing temporal information and traverses octree from both top and bottom for better compression ratio. Both these two works use recurrent neural network (RNN) to aggregate features but ignore spatial relation for each octant. VoxelContext-Net (Que, Lu, and Xu 2021) extracts voxel representation and utilizes 3D convolution based deep entropy model to compress nodes in octree. To further increase receptive field, OctAttention (Fu et al. 2022) gathers information from sibling and ancestor nodes in a fully autoregressive manner, and introduces attention mechanism for point cloud compression. Aside from the performance enhancement by this fully autoregressive model, the decoding complexity is greatly increased.

2.2 Efficient Context Model

As we stated above, the autoregressive context in octree-based DPCC greatly increases the decoding complexity ($> 900s$ per point cloud), which hinders the practical deployment of such methods. On the other hand, advancements in parallelizable autoregressive model in density estimation (Reed et al. 2017) and language models (Gu et al. 2017; Ghazvininejad et al. 2019) provide valuable insight for efficient context modeling in deep data compression. In the field of deep image compression, several works try to reduce decoding time by smartly design parallelizable autoregressive context model. Checkerboard context model (He et al. 2021) decodes half latent codes first and uses them as context for the other half. This idea is later adopted in deep video compression for fast decoding (Li, Li, and Lu 2022). ELIC (He et al. 2022) further improves channel context model by unevenly grouping. However, efficient parallelizable autoregressive context for DPCC is under-explored.

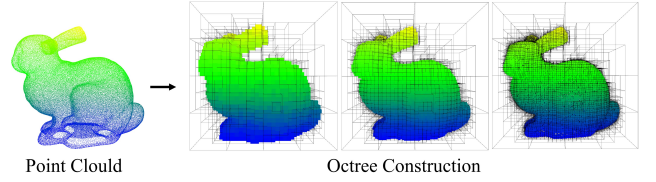


Figure 2: Point cloud BunnyMesh converted to octree with max depth of 5, 6, 7. The accuracy increases with the depth of octree. Octree-based context provides larger receptive field than voxel-based methods.

3 Methodology

3.1 Background: Octree-based Compression

Octree is a common data structure to describe 3D space (Huang et al. 2020); Each node of octree represents a cube in space. And each node can have eight cubic children that subdivide this node into eight trigrams. The occupancy code of a node is a binary flag to indicate spatial occupancy. An octree can be represented as the occupancy code sequence of every node. Formally, denote the occupancy code sequence of the whole octree as X , we have

$$X = \{x^1, \dots, x^l\} \quad (1)$$

where l is the total level of octree, and x^i is the occupancy code of level i . The sequence of occupancy codes $\{x^1, \dots, x^l\}$ could be used to reconstruct the octree losslessly. The essence of octree-based DPCC is to losslessly compress X . To achieve this, we use a model parameterized by θ to construct a parametric probability distribution $P_\theta(X)$ to approximate the true density $P(X)$. The smaller the KL divergence between the true density $P(X)$ and the predicted probability $P_\theta(X)$ is, the smaller the actual compressed bitrate $\mathbb{E}_{P(x)}[-\log P_\theta(X)]$ we can achieve. Thus, our optimization for bitrate is Eq. 2.

$$\theta^* \leftarrow \arg \min_{\theta} \mathbb{E}_{P(X)}[-\log P_\theta(X)] \quad (2)$$

The distortion of octree-based DPCC only comes from the conversion between octree and point cloud. During the construction of an octree with depth l , a point c_i in raw point cloud C is quantized into the nearest octree cube. While reconstructing octree back to point cloud \hat{C} , the coordinate of c_i is dequantized as the center of cube \hat{c}_i , which brings quantization error e . More specifically, e is bounded as Eq. 3, where w is the max length of leaf cubes, which is determined by l . A deeper octree indicates finer subdivision up to arbitrary precision (See Fig. 2) to achieve lossless compression.

$$e = \max_i \|\hat{c}_i - c_i\|_\infty \leq \frac{w}{2} \quad (3)$$

Naïvely constructing the density of $P_\theta(X)$ as a joint distribution is obviously intractable due to the extremely high dimension of X . Therefore, the key to octree compression is to construct a tractable factorization to $P_\theta(X)$ by utilizing the domain knowledge of dependency. A widely adopted

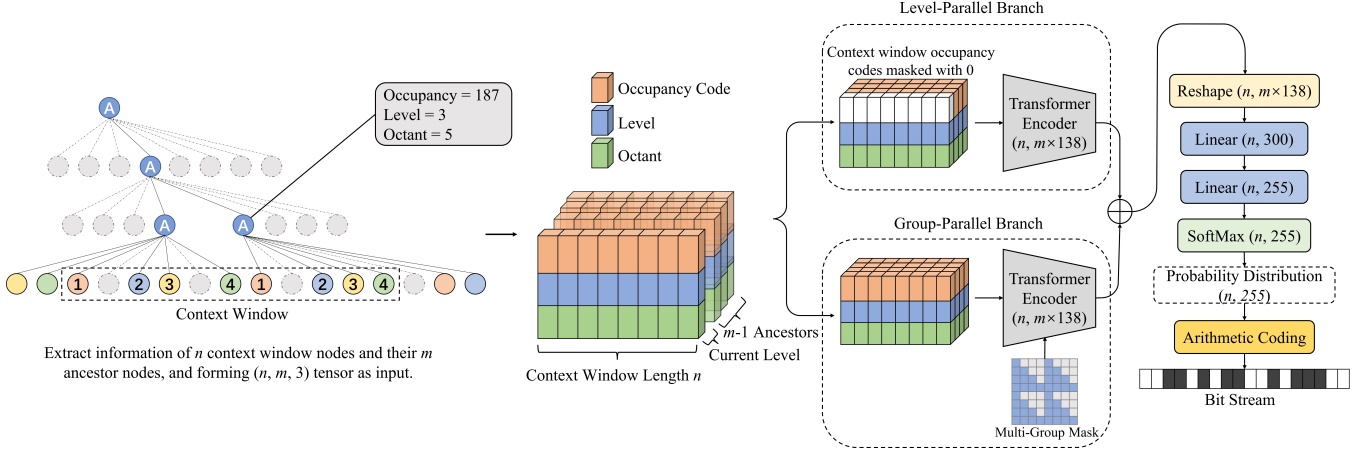


Figure 3: The overall architecture of ECM-OPCC.

factorization is the layer-wise autoregressive method (Huang et al. 2020):

$$P_{\theta}(X) = P_{\theta}(\mathbf{x}^1) \prod_{i=2}^l P_{\theta}(\mathbf{x}^i | \mathbf{x}^{<i}) \quad (4)$$

Moreover, previous works (Fu et al. 2022) use node level and position in parent node (octant) as auxiliary information to aid the prediction of occupancy codes. These auxiliary information in level i can be obtained from the occupancy code of previous level $i-1$. Formally, denote the auxiliary information of level i as \mathbf{y}^i , we have $\mathbf{y}^i = f(\mathbf{x}^{i-1})$. And the auxiliary information can be used to aid the layer-wise autoregressive model as Eq. 5,

$$P_{\theta}(X) = P_{\theta}(\mathbf{x}^1) \prod_{i=2}^l P_{\theta}(\mathbf{x}^i | \mathbf{x}^{<i}, \mathbf{y}^{\leq i}) \quad (5)$$

To fully exploit the context of ancestors and siblings, one can also adopt node-wise autoregression inside each layer \mathbf{x}^i to obtain a probabilistic model as Eq. 6, where N^i is the length of node in layer i , \mathbf{x}_j^i is the j^{th} node in i^{th} layer. And we call this type of model as fully autoregressive model.

$$P_{\theta}(\mathbf{x}^i | \mathbf{x}^{<i}, \mathbf{y}^{\leq i}) = P_{\theta}(\mathbf{x}_1^i | \mathbf{x}^{<i}, \mathbf{y}^{\leq i}) \prod_{j=2}^{N^i} P_{\theta}(\mathbf{x}_j^i | \mathbf{x}_{<j}^i, \mathbf{x}^{<i}, \mathbf{y}^{\leq i}) \quad (6)$$

In fact, the factorization described by Eq. 5 and Eq. 6 corresponds to the well-acknowledged SOTA of octree-based DPCC, named OctAttention (Fu et al. 2022). It achieves SOTA compression performance due to its thorough capture of context. However, the decoding of such model is fully sequential. In other words, the decoding time is proportional to $\Theta(\sum_i^l N^i)$, which can be extremely slow ($> 900s$ per point cloud).

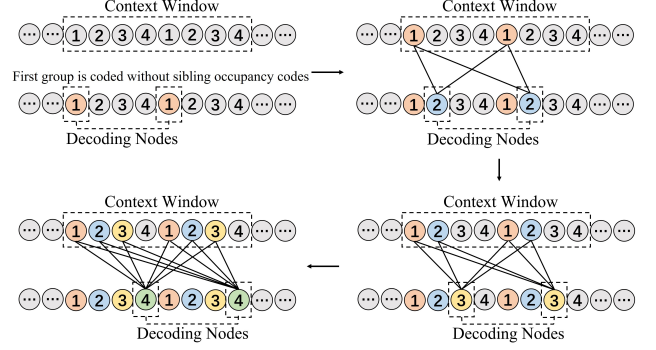


Figure 4: The decoding procedure of 4-group context window. Nodes within same group (marked with same ID) is decoded in parallel using nodes from previous groups as context.

3.2 Multi-Group Coding Strategy

As stated in Sec. 1, we propose a multi-group coding strategy to support large-scale context while greatly improve coding efficiency over fully autoregressive model (Fu et al. 2022) at the same time. Specifically, we compress layer i of octree autoregressively, with occupancy code $\mathbf{x}^{<i}$, level and octant $\mathbf{y}^{\leq i}$ from previous layers as context (See Fig. 3 and Eq. 6). Inside each layer, we divide the nodes into grouped context windows. Then we autoregressively encode each group of nodes, with previous groups inside the context window as context (See Fig. 4). The previous layer context (ancestor) and same layer context (siblings) are modeled by our dual transformer to estimate the likelihood for entropy coding. In this way, the decoding process between each context window and within each group is parallelizable, which greatly reduces decoding complexity. On the other hand, sufficient autoregressive modeling is maintained to promise compression performance.

Formally, denote the j^{th} window of nodes in layer i as $\mathbf{x}_{w_j}^i = \{\mathbf{x}_{w_j}^i, \dots, \mathbf{x}_{w_j}^i\}$, where g is the number of group,

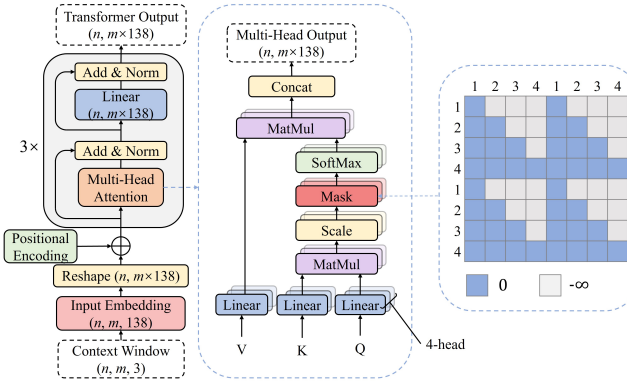


Figure 5: Transformer structure and multi-group mask matrix used in group-parallel branch. The network structure follows OctAttention (Fu et al. 2022). In this figure, the length of context window $n = 8$ and the group count $g = 4$. The blue blocks is 0 and gray blocks is $-\infty$.

n is the window size, h^i is the number of window in i^{th} layer. Then $\mathbf{x}_{w_j}^i$ is the k^{th} group nodes of j^{th} window in i^{th} layer, and we have the following factorization of layer-wise density:

$$P_\theta(\mathbf{x}^i | \mathbf{x}^{<i}, \mathbf{y}^{\leq i}) = \prod_{j=1}^{h^i} P_\theta(\mathbf{x}_{w_j}^i | \mathbf{x}^{<i}, \mathbf{y}^{\leq i}) \quad (7)$$

$$P_\theta(\mathbf{x}_{w_j}^i | \mathbf{x}^{<i}, \mathbf{y}^{\leq i}) = P_\theta(\mathbf{x}_{w_j}^i | \mathbf{x}^{<i}, \mathbf{y}^{\leq i}) \prod_{k=2}^g P_\theta(\mathbf{x}_{w_j}^i | \mathbf{x}_{w_j}^{i-k}, \mathbf{x}^{<i}, \mathbf{y}^{\leq i}) \quad (8)$$

And taking Eq. 7 and Eq. 8 back to the layer-wise autoregressive Eq. 5, we obtain the full likelihood model $P_\theta(X)$. To understand our design choice, we will discuss two questions:

- How multi-group coding affects decoding time?
- How multi-group coding affects the bitrate?

For the first question, let's assume that our hardware is fully parallelizable (e.g. infinitely number of kernels running at the same time). For fully autoregressive model, the decoding complexity is $\Theta(\sum_i^l N^i) = \Theta(|X|)$, where $|X|$ is the number of nodes in the octree. For our multi-group coding strategy, we have autoregressive dependency between layers. But for each context window inside each layer, the decoding is parallelizable. Moreover, although the decoding between groups inside context window is sequential, for each node inside each group, the decoding is also parallelizable. Thus, the decoding complexity is greatly reduced to $\Theta(l \cdot g)$. And empirically, as shown in Tab. 1, we also find our decoding time is greatly reduced over OctAttention (Fu et al. 2022), which is a fully autoregressive octree-based model.

For the second question, we can derive the theoretical bitrate as $\mathbb{E}_{P(X)}[-\log P(X)] + D_{KL}[P(X) || \hat{P}_\theta(X)]$ (See details in Appendix). And by applying the conclusion in Huang et al. (2022), we have the theoretical lowerbound on the bitrate as Tab. 2. Although the theoretical lowerbound of our method is higher than fully autoregressive method OctAttention, in practice we can achieve better bitrate by smartly design the model (See Sec. 3.3) and optimization (See Sec. 3.4).

	Asymptotic	Practical
fully autoregressive	$\Theta(\sum_{i=1}^l N^i)$	948s
Ours	$\Theta(lg)$	19.5s

Table 1: Asymptotic and practical decoding complexity between fully autoregressive model and our proposed multi-group coding strategy assuming fully parallelizable hardware. Experimental setup is described in Appendix.

	Theoretical Lowerbound	Practical
fully autoregressive	$\mathbb{E}[-\log P(X)]$	0.65 bpp
Ours	$\mathbb{E}[-\log P(X)] + \sum_{ij} \mathbb{H}(\mathbf{x}_{w_j}^i \mathbf{x}^{<i}) - \mathbb{H}(X)$	0.58 bpp

Table 2: Theoretical bitrate lowerbound and practical bitrate of fully autoregressive model and our proposed multi-group coding strategy. Experimental setup is described in Appendix.

3.3 Dual Transformer Structure

We design a dual branch transformer structure to support our coding strategy. Despite we state that our approach is fully autoregressive in layer level, in practice we trace back to at most $m - 1$ ancestors, where m is a hyper-parameter. It can be regarded as a m-Gram Markov chain. For each context window $\mathbf{x}_{w_j}^i$ in layer i , we trace back $m - 1$ ancestor nodes for each context window node (pad zero if not enough), to get $n \times m$ of sibling and ancestor nodes in total. We use occupancy code \mathbf{x} , level and octant \mathbf{y} as context to construct a $n \times m \times 3$ tensor as the input of transformer.

The level-parallel branch is designed to fully use all available information under the requirement that nodes in each level can be encoded and decoded in parallel. As shown in Fig. 3, the occupancy codes of current encoding/decoding level are masked with 0 to prevent information leakage (i.e., only already decoded information can be used for current node). In this branch, the information carried by occupancy code only comes from previous levels, which are ancestor nodes.

The group-parallel branch is designed to exploit context information carried by occupancy code of sibling nodes. As shown in Fig. 5, we use a multi-group mask matrix to modulate the attention layer, which ensures that only already de-

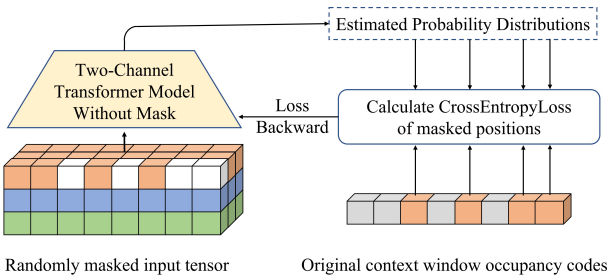


Figure 6: Overview of our pre-train strategy. We use same model without mask to process input, and only backward the loss at masked positions.

coded occupancy code from siblings can be used as context for current node. As explained in Fig. 4, nodes in different context windows or nodes in the same group can be encoded or decoded in parallel.

By combining these two branches, we fully implement the multi-group coding strategy described in Sec. 3.2. For encoding, we just need one forward pass of the two branches to compress all the nodes. For decoding, to decompress the node of each level, we need to run level-parallel branch once, and run group-parallel branch g times, so the total sequential-computation complexity is $\Theta(l \cdot g)$, as given in Tab. 1.

3.4 Random Masking Pretrain

The essential task of our transformer is to use context $x^{<i}, y^{<i}, x_{w_j}^i$ to predict the current group $x_{w_j}^i$. Therefore, it is important to fully exploit the predict ability of our transformer-based model. Inspired by BERT (Devlin et al. 2018), we design a pre-train method to help our model develop the ability of predicting current node with context information (See Fig. 6). Specifically, we randomly mask the input occupancy code with 50% probability, and use our model (without multi-group mask) to predict the masked positions with unmasked occupancy codes and full information of ancestors. This operation simulates the process of actual coding. As for gradient backward, we only backward the loss between predicted and ground truth occupancy codes of masked positions. We employ our pre-train method on object point cloud compression, and pre-trained for 2 epochs. We test our pre-train method on object dataset, and achieve considerable bpp improvement (See Tab. 4)

4 Experiment

4.1 Datasets

LiDAR Dataset For LiDAR dataset, we adopt SemanticKITTI (Behley et al. 2019), which is a large-scale outdoor-scene dataset for sparse point cloud semantic segmentation. It consists of 22 sequences, and contains a total of 43552 scans with 4549 million points.

Object Dataset For Object dataset, we adopt 8i Voxelized Full Bodies (MPEG 8i) (Killea et al. 2017) and Microsoft Voxelized Upper Bodies (MVUB) (Charles et al. 2016).

MPEG 8i contains sequences of smooth surface and complete human shape point clouds with 10 and 12bit precision. MVUB contains sequences of five half-body human shape dynamic voxelized point cloud with 9 and 10-bit precision.

To ensure fair comparison, we use the same train-test split as previous works (Fu et al. 2022; Que, Lu, and Xu 2021).

4.2 Implementation Details

Experimental Setup All experiments are performed on a machine with NVIDIA A100-PCIE-40GB GPU. We also test our method and OctAttention on the machine with one NVIDIA GeForce RTX 3090 for fair comparison with results reported in SparsePCGC (Wang et al. 2021). We use Adam optimizer with $lr = 10^{-3}$. It takes 2-4 days to train our model to 20 epochs. We tried different context window length n and group number g for ablation study. To balance compression bitrate and decoding time, we set $n = 1024, g = 8$ for LiDAR model and $n = 2048, g = 8$ for object model as default settings.

Baseline Methods In LiDAR point cloud lossy compression task, we set the maximum level of octree from 8 to 12 to achieve different R-D trade-off. We compare our work with SOTA octree-based compression method OctAttention (Fu et al. 2022), VoxelContext-Net (Que, Lu, and Xu 2021) OctSqueeze (Huang et al. 2020) and traditional hand-crafted G-PCC from MPEG standard in the stable version (TMC13 v14.0) (MPEG 2021). In object point cloud compression, we set the side length of the leaf cube to 1 to achieve lossless compression. We compare our method with G-PCC, OctAttention, and SOTA voxel-based method SparsePCGC (Wang et al. 2021), VoxelDNN (Nguyen et al. 2021a), MSVoxelDNN (Nguyen et al. 2021b). We apply lossless compression on above methods for fair comparison on bpp and encoding/decoding time.

Training and Testing Strategy Following previous octree-based works, we train 2 separate model on LiDAR and object datasets. For LiDAR task, we construct the training point cloud to 12-level octree so that our model can learn the distribution at all level in one training procedure. We truncate the octree to 8-12 levels to test our model at different bitrates. For object point clouds, we construct them losslessly to octree for training and testing.

Evaluation Metrics For fair comparison, we adopt same evaluation metrics with previous works (Fu et al. 2022; Que, Lu, and Xu 2021). Specifically, for LiDAR, we use point-to-point (D1 PSNR), point-to-plane (D2 PSNR) and chamfer distance (CD) to measure reconstruction quality in lossy compression. We compare bpp, encoding time and decoding time to evaluate compression performance. The results of compared works are performed on machines with the same GPU configuration. All bpp data are obtained by averaging over sequence.

4.3 Experimental Results

Lossy Compression Performance on LiDAR The bpp-distortion curves of LiDAR point cloud compression is shown in Fig. 7. Our model outperforms other methods at

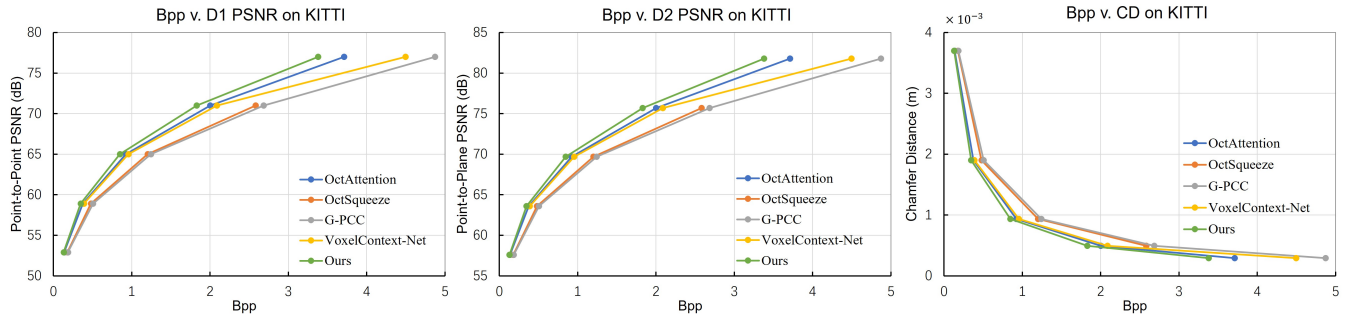


Figure 7: Results of different methods on SemanticKITTI dataset.

all bitrates consistently. Specifically, we save 31% bitrate over G-PCC averagely over five distortion levels. We also achieve 8.9% and 4.4% relative reduction at high and low bitrate respectively versus SOTA method OctAttention. Experimental results verify the effectiveness of our multi-group context model over previous deep learning works and traditional method.

Lossless Compression Performance on Object The lossless compression results on object datasets are shown in Table 3, our method saves 42.4% and 33.6% bpp averagely on MPEG 8i and MVUB over traditional method G-PCC. Specifically, we compare our method w/ and w/o pre-trained model. Tab. 4 shows that our method w/ pre-train outperforms OctAttention by 6.3% and 1.3% on two datasets, and gets considerable gains over models w/o pre-train.

Point Cloud	bpp			Gain*
	G-PCC	OctAttention	Ours	
<i>MPEG 8i</i>				
Loot10	0.95	0.62	0.55	42.1%
Redandblack10	1.09	0.73	0.66	39.4%
Boxer9	0.96	0.60	0.53	45.3%
Boxer10	0.94	0.59	0.51	
Thaidancer9	0.99	0.64	0.59	40.9%
Thaidancer10	0.99	0.65	0.58	
Average	0.99	0.64	0.57	42.4%
<i>MVUB</i>				
Phil9	1.23	0.83	0.79	35.8%
Phil10	1.07	0.79	0.76	29.0%
Ricardo9	1.04	0.79	0.76	34.6%
Ricardo10	1.07	0.72	0.69	35.5%
Average	1.10	0.76	0.73	33.6%

Table 3: Lossless compression results of different methods on MPEG 8i and MVUB datasets. * The bpp saving over G-PCC.

Encoding and Decoding Efficiency on Object We adopt MPEG 8i dataset to compare encoding and decoding efficiency. And we compare our results against G-PCC, voxel-based SOTA method SparsePCGC (Wang et al. 2021),

Point Cloud	Ours (w/o pre-train)		Ours (w/ pre-train)	
	bpp	Gain*	bpp	Gain*
MPEG 8i	0.61	4.7%	0.60	6.3%
MVUB	0.77	-1.3%	0.75	1.3%

Table 4: Ablation study of lossless compression on MPEG 8i and MVUB dataset. * The bpp saving over OctAttention.

VoxelDNN(Nguyen et al. 2021a), and octree-based SOTA method OctAttention (Fu et al. 2022). As shown in Tab. 5, our method outperforms other deep learning methods in compression performance, and saves 98% of decoding time compared with OctAttention. The encoding time of our method is slower than Octattention due to the dual transformer structure. Moreover, a scatter plot of bpp and decoding time is shown in Fig. 1. It can be seen that our method achieves SOTA compression performance with very fast decoding time.

4.4 Ablation Study and Analysis

Dual Branch Transformer To explore the effectiveness of our dual branch transformer, we separate the two branches into independent models and test them separately. We adopt MPEG 8i dataset and test average bpp, encoding time, total decoding time and neural network inference time to evaluate the performance. We set context window length $n = 2048$ and group count $g = 8$ for group-parallel branch, we train 20 epochs for each model. Tab. 6 demonstrates that the bitrate results obtained by the separate models are worse than the dual model. Meanwhile, both branches are marginally accelerated in decoding, as the size of neural network is reduced. The level-parallel branch can decode the context window in parallel, so that the running time of neural network is negligible. Experimental results verify that the dual branch approach is important to compression performance while brings only marginal decoding time overhead.

Effect of Context Window Length We set the context window length $n \in \{128, 256, 512, 1024, 2048, 4096\}$ to study the effect of n . For each model we set group count $g = 8$ and train 20 epochs. And all other parameters remain the same. Tab. 7 shows we obtain 12.1% reduction on bitrate

Point Cloud	Traditional		Voxel-based		Octree-based	
	G-PCC*	SparsePCGC*	VoxelDNN*	MSVoxelDNN*	OctAttention	Ours
loot_vox10 (bpp)	0.95	0.63	0.58	0.73	0.62	0.55
redandblack_vox10 (bpp)	1.09	0.72	0.66	0.87	0.73	0.66
boxer_viewdep_vox10 (bpp)	0.94	0.60	0.55	0.70	0.59	0.51
Thaidancer_viewdep_vox10 (bpp)	0.99	0.67	0.68	0.85	0.65	0.58
Average bpp	0.99	0.66	0.62	0.79	0.65	0.58
Average Gain over G-PCC	-	33.8%	37.6%	20.5%	34.6%	41.9%
Average Encoding Time (s)	4.0	9.5	885	54	0.80	1.92
Average Decoding Time (s)	1.0	9.1	640	58	948	19.5

Table 5: Bpp and coding time results on MPEG 8i dataset compared with G-PCC, voxel-based SOTA and octree-based SOTA methods. The data with * comes from Wang et al. (2021).

Branch	Avg. bpp on MPEG 8i	Encoding time (s)	Decoding time (s)	
			Total	Network
Level (L)	0.75	0.79	7.2	0.8
Group (G)	0.64	0.82	9.4	4.0
Dual (L+G)	0.58	1.43	11.7	6.9

Table 6: Independent performance of two branches on object dataset MPEG 8i.

n	Avg. bpp on MPEG 8i	Encoding time (s)	Decoding time (s)	
			Total	Network
128	0.66	10.8	98.8	84.3
256	0.66	5.54	55.0	44.1
512	0.61	2.68	29.9	22.5
1024	0.59	1.46	16.4	11.0
2048	0.58	1.43	11.7	6.9
4096*	-	-	-	-

Table 7: Performance of bpp and coding time on object datatset MPEG 8i when using various context window length. * We can not provide result with $n = 4096$, as it exceeds 40G GPU memory while training.

by enlarging n from 128 to 2048. Moreover, because expanding the context size n can reduce the number of forward pass and enable our device to process data continuously, we reduce the encoding time by 7.5 times, and decoding time by 8.4 times. And we also reduce neural network inference time decreases by 12 times while decoding. Therefore, enlarging context window will be more effective and also more efficient in our method. Therefore for all above results, we set $n = 2048$ for best performance under the constrain of GPU memory.

Effect of Group Count We also study the effect of group count g on the performance of our coding strategy. We set group count $g = \{2, 4, 6, 8, 16, 32\}$, $n = 2048$ and train the model for 20 epochs. Tab. 8 demonstrates that we save 13.6% bitrate by increasing group count from 2 to 32. This is

because as the group count increases, more occupancy codes of sibling nodes can be used as guiding information by latter groups. The encoding time remains similar, as the encoding procedure is parallel within each context window. Also, because the decoding procedure is sequentially conducted by group, the decoding time shows a multiple upward trend with the increase of group count. It is also noteworthy that when $g \geq 8$, the gain in bpp becomes only marginal while the increment in decoding time becomes significant. We set $g = 8$ as it is a sweet-spot with reasonably good compression performance and fast decoding time.

g	Avg. bpp on MPEG 8i	Encoding time (s)	Decoding time (s)	
			Total	Network
2	0.66	1.38	7.9	2.6
4	0.61	1.30	8.8	3.6
8	0.58	1.43	11.7	6.9
16	0.57	1.26	19.2	13.6
32	0.57	1.37	33.3	26.6

Table 8: Performance of bpp and coding time on object datatset MPEG 8i when using various group count.

5 Conclusion

In this work, We propose an efficient large-scale context entropy model for point cloud geometry compression. To be specific, we propose a multi-group coding strategy to encode and decode the octree efficiently, based on which we propose a dual transformer architecture. We also design a random masking pre-train strategy. Results show that our model achieves SOTA compression performance, and reduce decoding time by up to 98% compared to previous octree-based works, which makes the practical deployment of octree-based DPCC possible.

6 Discussion

The compression rate improvement over previous SOTA method on MVUB dataset is marginal compared with those

on MPEG 8i and SemanticKITTI. It is unclear why the compression rate improvement on the three considered datasets is different. We leave this for future investigation.

References

Behley, J.; Garbade, M.; Milioto, A.; Quenzel, J.; Behnke, S.; Stachniss, C.; and Gall, J. 2019. SemanticKITTI: A Dataset for Semantic Scene Understanding of LiDAR Sequences. *IEEE/CVF International Conference on Computer Vision (ICCV)*, 9296–9306.

Biswas, S.; Liu, J.; Wong, K.; Wang, S.; and Urtasun, R. 2020. MuSCLE: Multi Sweep Compression of LiDAR using Deep Entropy Models. In Larochelle, H.; Ranzato, M.; Hadsell, R.; Balcan, M.; and Lin, H., eds., *Advances in Neural Information Processing Systems*, volume 33, 22170–22181. Curran Associates, Inc.

Cao, C.; Preda, M.; and Zaharia, T. 2019. 3D point cloud compression: A survey. In *The 24th International Conference on 3D Web Technology*, 1–9.

Charles, L.; Qin, C.; Sergio, O. E.; and Philip, A. C. 2016. Microsoft voxelized upper bodies - a voxelized point cloud dataset. *ISO/IEC JTC1/SC29 Joint WG11/WG1 (MPEG/JPEG) input document m38673/M7201*.

Devlin, J.; Chang, M.-W.; Lee, K.; and Toutanova, K. 2018. BERT: Pre-training of Deep Bidirectional Transformers for Language Understanding.

Fu, C.; Li, G.; Song, R.; Gao, W.; and Liu, S. 2022. OctAttention: Octree-based Large-scale Contexts Model for Point Cloud Compression. *arXiv preprint arXiv:2202.06028*.

Ghazvininejad, M.; Levy, O.; Liu, Y.; and Zettlemoyer, L. 2019. Mask-predict: Parallel decoding of conditional masked language models. *arXiv preprint arXiv:1904.09324*.

Gu, J.; Bradbury, J.; Xiong, C.; Li, V. O.; and Socher, R. 2017. Non-autoregressive neural machine translation. *arXiv preprint arXiv:1711.02281*.

He, D.; Yang, Z.; Peng, W.; Ma, R.; Qin, H.; and Wang, Y. 2022. Elic: Efficient learned image compression with unevenly grouped space-channel contextual adaptive coding. In *Proceedings of the IEEE/CVF Conference on Computer Vision and Pattern Recognition*, 5718–5727.

He, D.; Zheng, Y.; Sun, B.; Wang, Y.; and Qin, H. 2021. Checkerboard context model for efficient learned image compression. In *Proceedings of the IEEE/CVF Conference on Computer Vision and Pattern Recognition*, 14771–14780.

Huang, F.; Tao, T.; Zhou, H.; Li, L.; and Huang, M. 2022. On the Learning of Non-Autoregressive Transformers. In Chaudhuri, K.; Jegelka, S.; Song, L.; Szepesvari, C.; Niu, G.; and Sabato, S., eds., *Proceedings of the 39th International Conference on Machine Learning*, volume 162 of *Proceedings of Machine Learning Research*, 9356–9376. PMLR.

Huang, L.; Wang, S.; Wong, K.; Liu, J.; and Urtasun, R. 2020. OctSqueeze: Octree-Structured Entropy Model for LiDAR Compression. In *Proceedings of the IEEE/CVF Conference on Computer Vision and Pattern Recognition (CVPR)*.

Killea, R.; Li, Y.; Bastani, S.; and McLachlan, P. 2017. 8i Voxelized Full Bodies - A Voxelized Point Cloud Dataset. *ISO/IEC JTC1/SC29 Joint WG11/WG1 (MPEG/JPEG) input document WG11M40059/WG1M74006*.

Li, J.; Li, B.; and Lu, Y. 2022. Hybrid Spatial-Temporal Entropy Modelling for Neural Video Compression. *arXiv preprint arXiv:2207.05894*.

Liang, Z.; and Liang, F. 2022. TransPCC: Towards Deep Point Cloud Compression via Transformers.

MPEG. 2021. <https://github.com/MPEGGroup/mpeg-pcc-tmc13>.

Nguyen, D. T.; Quach, M.; Valenzise, G.; and Duhamel, P. 2021a. Learning-based lossless compression of 3d point cloud geometry. In *ICASSP 2021-2021 IEEE International Conference on Acoustics, Speech and Signal Processing (ICASSP)*, 4220–4224. IEEE.

Nguyen, D. T.; Quach, M.; Valenzise, G.; and Duhamel, P. 2021b. Multiscale deep context modeling for lossless point cloud geometry compression. In *2021 IEEE International Conference on Multimedia & Expo Workshops (ICMEW)*, 1–6. IEEE.

Que, Z.; Lu, G.; and Xu, D. 2021. Voxelcontext-net: An octree based framework for point cloud compression. In *Proceedings of the IEEE/CVF Conference on Computer Vision and Pattern Recognition*, 6042–6051.

Reed, S.; van den Oord, A.; Kalchbrenner, N.; Colmenarejo, S. G.; Wang, Z.; Chen, Y.; Belov, D.; and de Freitas, N. 2017. Parallel Multiscale Autoregressive Density Estimation. In Precup, D.; and Teh, Y. W., eds., *Proceedings of the 34th International Conference on Machine Learning*, volume 70 of *Proceedings of Machine Learning Research*, 2912–2921. PMLR.

Tu, C.; Takeuchi, E.; Carballo, A.; and Takeda, K. 2019. Point cloud compression for 3d lidar sensor using recurrent neural network with residual blocks. In *2019 International Conference on Robotics and Automation (ICRA)*, 3274–3280. IEEE.

Wang, J.; Ding, D.; Li, Z.; Feng, X.; Cao, C.; and Ma, Z. 2021. Sparse Tensor-based Multiscale Representation for Point Cloud Geometry Compression. *arXiv preprint arXiv:2111.10633*.

You, K.; and Gao, P. 2021. Patch-Based Deep Autoencoder for Point Cloud Geometry Compression. In *ACM Multimedia Asia*, 1–7.